Pediatr Radiol (2017) 47:146–153
DOI 10.1007/s00247-016-3729-1

ORIGINAL ARTICLE

Magnetic resonance imaging of pulmonary infection in immunocompromised children: comparison with multidetector computed tomography

H. Nursun Ozcan[1] · Ayşegul Gormez[1] · Yasemin Ozsurekci[2] · Jale Karakaya[3] · Berna Oguz[1] · Sule Unal[4] · Mualla Cetin[4] · Mehmet Ceyhan[2] · Mithat Haliloglu[1]

Received: 29 May 2016 / Revised: 28 August 2016 / Accepted: 7 October 2016 / Published online: 28 October 2016
© Springer-Verlag Berlin Heidelberg 2016

Abstract
Background Computed tomography (CT) is commonly used to detect pulmonary infection in immunocompromised children.
Objective To compare MRI and multidetector CT findings of pulmonary abnormalities in immunocompromised children.
Materials and methods Seventeen neutropaenic children (6 girls; ages 2-18 years) were included. Non-contrast-enhanced CT was performed with a 64-detector CT scanner. Axial and coronal non-enhanced thoracic MRI was performed using a 1.5-T scanner within 24 h of the CT examination (true fast imaging with steady-state free precession, fat-saturated T2-weighted turbo spin echo with motion correction, T2-weighted half-Fourier single-shot turbo spin echo [HASTE], fat-saturated T1-weighted spoiled gradient echo). Pulmonary abnormalities (nodules, consolidations, ground glass opacities, atelectasis, pleural effusion and lymph nodes) were evaluated and compared among MRI sequences and between MRI and CT. The relationship between MRI sequences and nodule sizes was examined by chi- square test.
Results Of 256 CT lesions, 207 (81%, 95% confidence interval [CI] 76–85%) were detected at MRI. Of 202 CT-detected nodules, 157 (78%, 95% CI 71–83%) were seen at motion-corrected MRI. Of the 1–5-mm nodules, 69% were detected by motion-corrected T2-weighted MRI and 38% by HASTE MRI.
Conclusion Sensitivity of MRI (both axial fat-saturated T2-weighted turbo spin echo with variable phase encoding directions (BLADE) images and HASTE sequences) to detect pulmonary abnormalities is promising.

Keywords Children · Consolidation · Computed tomography · Detection rate · Immunosuppression · Lung · Lung nodules · Magnetic resonance imaging · Pulmonary infection

Introduction

Pulmonary infections are serious causes of morbidity and mortality in iatrogenic immunocompromised children. Chest radiography is the first imaging modality for evaluation of pulmonary infections. However, due to their low sensitivity, chest radiographs may be normal or show minimal nonspecific abnormalities only [1]. Hence, CT is accepted as an important imaging modality for the detection and characterization of pulmonary nodules and infections [2]. Recent studies demonstrated the utility of lung MRI with different sequences in focal lung lesions, infiltrative lung diseases and metastases in adults [3–7]. Further studies compare the lung MRI findings with those of multidetector CT (MDCT) in immunocompromised adults [8–11]. In the pediatric literature, there are only a few pilot studies of lung MRI [12–17], performed in otherwise healthy children using routine sequences. The purpose of our study was to compare MRI and MDCT findings in pulmonary abnormalities in immunocompromised children.

✉ Mithat Haliloglu
mithath@hacettepe.edu.tr

[1] Department of Radiology, Hacettepe University School of Medicine, Sihhiye, 06100 Ankara, Turkey

[2] Department of Pediatric Infectious Disease, Hacettepe University School of Medicine, Ankara, Turkey

[3] Department of Biostatistics, Hacettepe University School of Medicine, Ankara, Turkey

[4] Department of Pediatric Hematology, Hacettepe University School of Medicine, Ankara, Turkey

Materials and methods

Patients

Between April 2014 and April 2015, 17 neutropenic children (6 girls; mean age: 9.5 years; range: 2–18 years) were included in this prospective study. All of the patients had hematological malignancies (acute myeloid leukemia in nine, acute lymphatic leukemia in eight). Clinical and demographic characteristics, medical history, laboratory and radiologic findings, type and antimicrobial susceptibility of the isolated microorganisms, and outcome of the patients were noted. The study was reviewed and approved by our University Institutional Ethics Committee (number: GO 14/79). After patients' parents/legal guardians had given informed consent, the patients were enrolled in the study.

All of our patients were considered at high risk for invasive fungal disease according to the criteria, including acute myeloid leukemia, relapsed acute lymphatic leukemia, allogeneic hematopoietic stem-cell transplantation recipients with persistent fever (≥96 h) despite broad-spectrum antibiotic treatment, and expected prolonged neutropenia (>10 days) [18]. Respiratory symptoms and signs including cough, sputum production, thoracic pain, dyspnea, hemoptysis or the presence of a pleural rub in a high-risk patient were considered suggestive for the diagnosis of invasive fungal disease [19]. For a patient with appropriate host factors and clinical evidence of pulmonary disease, we performed some radiologic studies (chest radiography, CT, MRI) to find clues for the diagnosis of invasive fungal disease and mycological studies (microscopy/culture of sputum, bronchoalveolar lavage fluid, any clinical specimens and/or serum galactomannan antigen detection) to uncover mycological evidence. The patients were classified as having possible, probable and proven fungal infection according to the proposed criteria of the European Organization for Research and Treatment of Cancer/Mycosis Study Group consensus working party [20]. Chest MRI was performed in all patients within 24 h of the MDCT. Patients with standard medical contraindications to MR examination (e.g., cochlear implant), children requiring sedation and patients in whom MDCT and MR examination could not be performed within the same 24 h were excluded.

CT protocol

Non-enhanced CT was performed with a 64-MDCT scanner (Somatom Definition 64; Dual Source, Siemens Medical Solutions, Erlangen, Germany) at 5-mm section thickness, pitch of 1, 2-mm reconstructed section thickness, weight-based kilo voltage, low-dose tube current and high-speed mode. Imaging volume was extended from pulmonary apex to costophrenic angle. Images were reconstructed with both lung (window width, 1,500 Hounsfield units (HU); window level, -500 HU) and soft-tissue kernel (window width, 450 HU; window level, 60 HU). Patients with absence of nodules in MDCT imaging were not excluded from the study in order to analyze false-positive lesions at MR examination.

MRI protocol

Thoracic MRI without contrast administration was performed in all patients using a 1.5-T MR imaging scanner (Symphony TIM; Siemens, Erlangen, Germany) coil system. Images were obtained in axial and coronal planes with coronal true fast imaging with steady-state free precession, axial fat-saturated T2-weighted turbo spin echo with variable phase encoding directions (BLADE), axial T2-weighted half-Fourier acquisition single-shot turbo spin-echo (HASTE), axial fat-saturated T1-weighted volumetric interpolated breath-hold examination (VIBE) and axial fat-saturated T1-weighted fast low-angle shot gradient echo (FLASH). Table 1 demonstrates the sequences parameters. Imaging time was about 9 min for axial sequences and coronal 21 s for the coronal sequence, in total about 10 min. Sedation was not applied to any of the patients. Instead, MRI was performed during sleep for children younger than 5 years old, with respiratory gating to reduce motion artifact.

Image analysis

Two radiologists with 10 years (HNO) and 5 years (AG) of experience in interpreting pediatric thoracic MDCT and MR images first evaluated the images of each patient independently. Then, the radiologists evaluated the images together and reached a final decision in consensus. MDCT was considered

Table 1 Chest MRI sequence parameters

Parameters[a]	T2-weighted BLADE	HASTE	VIBE	FLASH
TR/TE (ms)	4,845.2/90	1,020/92	4.9/2.4	270/2.6
Flip angle (degrees)	140	133	10	70
Field of view (mm)	350x350	350x273.4	380x285	380x285
Slice thickness (mm)	5	6	2	6

[a] All images were obtained in the transverse plane

BLADE turbo spin echo with variable phase encoding directions, *FLASH* fast low-angle shot (gradient echo), *HASTE* half-Fourier single-shot turbo spin echo, *VIBE* volume-interpolated breath-hold (gradient echo) imaging

the reference standard for the diagnosis. All images were analyzed retrospectively. Reviewers first examined the MR images in order not to be affected by the reference standard. CT images were evaluated in a different session at least 10 days later to reduce bias. Additionally, the images were randomly evaluated masked to patient identity.

Standard nomenclature for pulmonary parenchymal CT findings was used to denominate the lesions. The same definitions were used for MRI as well, since there are not any up-to-date imaging criteria specifically for MRI. A round opacity, at least moderately well marginated, with a diameter of 3 cm or smaller was defined as a nodule. A hazy increased attenuation at CT or an area of hyperintensity that preserves the bronchovascular margins in MRI was defined as ground-glass opacity. A homogeneous increase in lung parenchyma attenuation that obscures the margins of vessels and airway walls was defined as consolidation [21]. Nodules, ground-glass opacity and consolidation were evaluated at CT and all four MR sequences. Also presence of atelectasis, pleural effusion, hilar and mediastinal lymph node was noted by reviewing CT images, BLADE images and HASTE sequences.

Each lesion was localized to exist in the right upper lung, right middle lung, right lower lobe, left upper lobe and left lower lobe. CT and MR imaging findings were examined by the two observers in consensus for the presence, number and size of nodules, presence and number of consolidations, ground-glass opacity, atelectasis, pleural effusion and lymph nodes. Nodules were classified by size as 1-5 mm (group 1), 6-10 mm (group 2) and >10 mm (group 3).

Statistical analysis

Data analysis was performed by IBM SPSS Statistics 21.0 software package (IBM Corp., Armonk, NY, USA). We assessed the sensitivity of different MR sequences for the detection of lesions; 95% confidence interval for MRI sensitivity was calculated. Cochran Q test was used to compare the effectiveness of different MR sequences. Differences between any two sequences were tested using the McNemar test with Bonferroni corrections. Relationship between MR sequences and nodule size was examined by chi-square test (Pearson chi-square and Fisher exact test). Statistical significance was set at $P < 0.05$.

Results

Two patients were diagnosed with probable and 15 with possible invasive fungal disease. One of the patients who was classified as probable invasive fungal disease had positive serum galactomannan antigen test and the other had *Aspergillus fumigatus* complex in sputum culture in addition to the presence of a host factor and a clinical criterion. The following infectious pathogens were found in catheter and/or blood cultures among the remaining patients: *Escherichia coli, Klebsiella oxytoca* and *Staphylococcus aureus*.

Imaging findings

All CT and MR examinations were performed without any complications and all of the images were accepted diagnostic in terms of image quality. A total of 85 lung lobes in 17children were evaluated to detect the presence and characteristics of abnormalities on CT and MR images. All of the patients had at least one of the pulmonary abnormalities (nodule, ground-glass opacity, consolidation, atelectasis, lymph node, pleural effusion) at both CT and MR images.

A total of 256 lesions were detected at CT and 207 of these were detected by MRI. The sensitivity of MRI for detection of pulmonary abnormality was hence 81% (95% confidence interval [CI] 76–85%). Table 2 summarizes the radiologic findings detected on CT and MRI.

In 12/17 patients (71%), nodules were detected on CT images, and each of these 12 also has nodules detected on MRI. In 12/17 patients (71%), ground-glass opacity was detected on CT images; 10/12 also had ground-glass opacity detected on MR images. In 6/17 patients (35%), consolidation was detected on CT images, and each of these 6 also had consolidation detected at MRI. Table 3 summarizes the detection sensitivity of four different MRI sequences for nodule, ground-glass opacity and consolidation.

Table 2 Detection sensitivity of MRI for all types of lesions detected on CT

Lesion type (number of lesions on CT)	Number of lesions on MRI	MRI sensitivity 95% confidence interval
Nodule (202)	157	71—83%
Ground glass opacity (20)	16	56—94%
Consolidation (8)	8	63—100%
Atelectasis (9)	9	66—100%
Pleural effusion (5)	5	48-100%
Lymph nodes (12)	12	74—100%
Any lesion (256)	$n = 207$	75—85%

Table 3 Sensitivity of four different MRI sequences for nodule, ground glass opacity and consolidation

	T2-BLADE		HASTE		VIBE		FLASH		
Type of lesion (number detected on CT)	Number of lesions detected	95% confidence interval for sensitivity	Number of lesions detected	95% confidence interval for sensitivity	Number of lesions detected	95% confidence interval for sensitivity	Number of lesions detected	95% confidence interval for sensitivity	*P**
Nodule (202)	157	72—83%	111	48—61%	61	23—36%	48	17—29%	<0.001
Ground glass opacity (20)	16	62—97%	16	62—97%	0	0—17%	0	0—17%	<0.001
Consolidation (8)	8	67—100%	7	52—97%	7	52—97%	7	52—97%	0.39

* Cohran Q test results

BLADE turbo spin echo with variable phase encoding directions, *FLASH* fast low-angle shot (gradient echo), *HASTE* half-Fourier single-shot turbo spin echo, *VIBE* volume-interpolated breath-hold (gradient echo) imaging

Nodules

A total of 202 nodules were detected in 12 patients on reference standard CT imaging (Fig. 1). Among them, 157 nodules were seen at MRI with a sensitivity of 78% (95% CI 72–83%) on BLADE images, 55% (95% CI 48–61%) on HASTE, 30% (95% CI 24–37%) on VIBE and 24% (95% CI 18–30%) in FLASH sequences, respectively, independently of their size.

The detection rate for nodules ≤5 mm was significantly higher on BLADE compared to HASTE sequences ($P < 0.001$; Fig. 2). Table 4 demonstrates in detail the differences in the sensitivities of sequences according to nodule size.

In one patient, one more group 3 nodule was detected on both BLADE images and HASTE sequences. In another patient, three group 2 and 10 group 1 nodules were false-positive

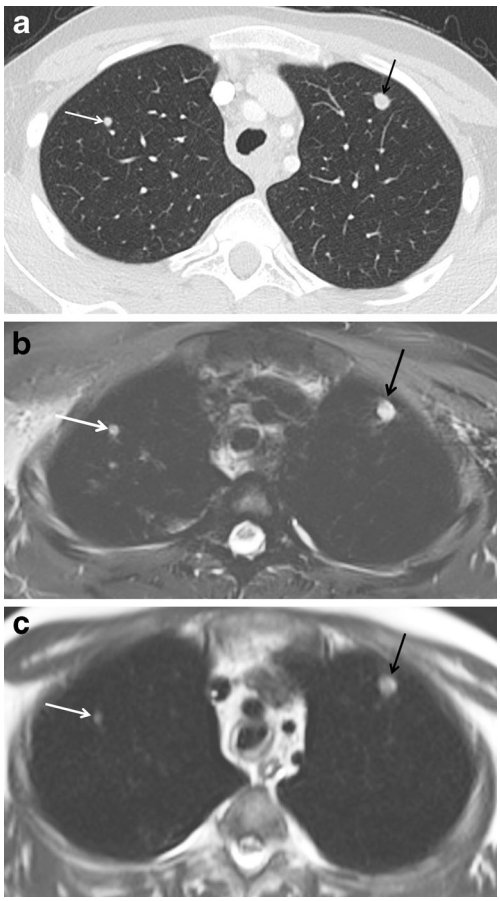

Fig. 1 A 17-year-old boy with acute lymphoblastic leukemia. **a** Transverse thin-section CT image shows a 4.5-mm nodule in the upper lobe of right lung (*white arrow*) and an 8-mm nodule in the upper lobe of left lung (*black arrow*). The two nodules can be visualized at MRI both on transverse T2-weighted spin echo with periodically rotated k space trajectory (**b**; annotation as in [**a**]) and on T2-weighted half-Fourier single-shot turbo spin echo (**c**; annotation as in [**a**])

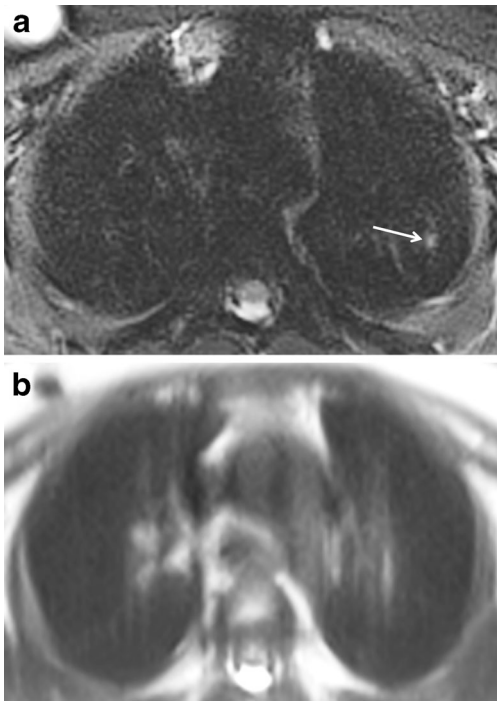

Fig. 2 A 9-year-old boy with acute lymphoblastic leukemia. **a** Transverse T2-weighted T2-weighted spin echo with periodically rotated k space trajectory demonstrates a nodule in the upper lobe of left lung (*arrow*). **b** Transverse T2-weighted half-Fourier single-shot turbo spin echo at the same level does not demonstrate the lesion

Table 4 Sensitivity of four different MRI sequences by CT-determined nodule size

	T2-BLADE		HASTE		VIBE		FLASH	
Nodule size (number detected on CT)	Number of lesions detected	95% confidence interval for sensitivity	Number of lesions detected	95% confidence interval for sensitivity	Number of lesions detected	95% confidence interval for sensitivity	Number of lesions detected	95% confidence interval for sensitivity
1–5 mm (146)	101	61—76%	55	29—45%	25	11—23%	21	5—20%
6–10 mm (49)	49	92—100%	49	92—100%	31	49—75%	22	31—58%
>10 mm (7)	7	64—100%	7	64—100%	5	35—91%	5	35—91%
*P value	<0.001		<0.001		<0.001		<0.001	

* chi-square test results

BLADE turbo spin echo with variable phase encoding directions, *FLASH* fast low-angle shot (gradient echo), *HASTE* half-Fourier single-shot turbo spin echo, *VIBE* volume-interpolated breath-hold (gradient echo) imaging

on BLADE images. Also, four nodules were defined as group 2 on HASTE whereas they were identified as group 1 on CT images. In one patient, the total number of nodules matched with CT: 6 nodules defined as group 2 on both BLADE and HASTE sequences, but as group 1 on CT. The nodule detection capability was significantly different among the set of sequences ($P < 0.001$). Every pairwise comparison was significantly different except VIBE and FLASH sequences.

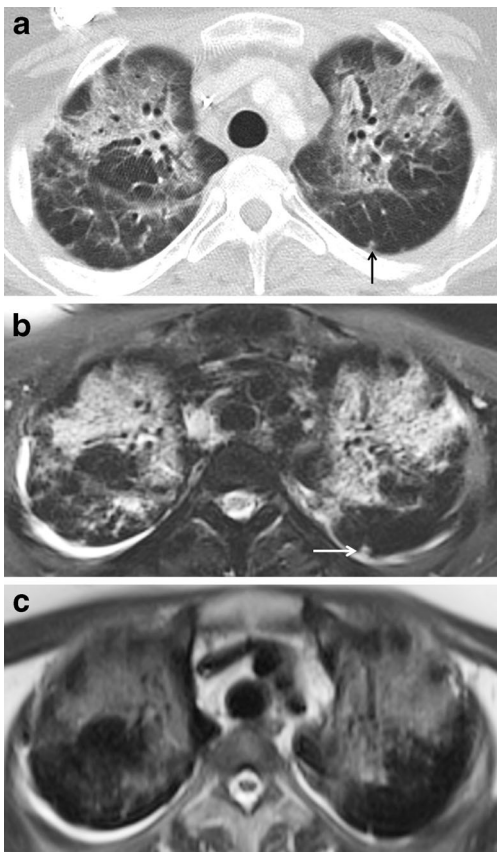

Fig. 3 A 16-year-old boy with acute lymphoblastic leukemia. **a** Transverse thin-section CT image shows bronchiectasis, ground glass opacity in both the upper lobes of lung and subpleural nodule (*arrow*) in the lower lobe of left lung. The bronchiectasis and groundglass opacity in both the upper lobes of lung can be visualized on corresponding transverse T2-weighted spin echo with periodically rotated k space trajectory (BLADE; **b**) and transverse T2-weighted half-Fourier single-shot turbo spin echo MRI **(c)**. Note that subpleural nodule in the lower lobe of left lung is better demonstrated on BLADE sequence (*arrow* in **b**)

Ground-glass opacity

A total of 20 ground-glass opacities were seen on CT in 12 patients. Among them, in two patients, ground-glass opacity was absent on MRI and 16 ground-glass opacities were detected on MRI with a sensitivity of 80% (95% CI 63-98%). These were all detected only on BLADE and HASTE sequences (Figs. 3 and 4). In one patient, false-positive presence of ground-glass opacity at HASTE sequences was observed. Also, in two patients, false-positive ground-glass opacities were seen on both HASTE and BLADE images. Since there

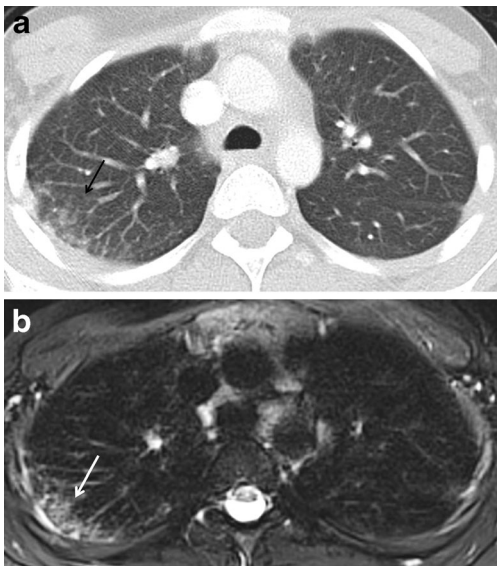

Fig. 4 An 11-year-old girl with acute lymphoblastic leukemia. **a** Transverse thin-section CT image shows ground glass opacity (*arrow*) in the upper lobe of right lung. **b** Corresponding transverse T2-weighted spin echo with periodically rotated k space trajectory MRI also demonstrates the lesion (*arrow*)

were multiple nodules and ground-glass opacities on other lobes, MRI would have been sufficient for correct diagnosis in these patients.

Consolidation

Eight consolidations were seen on CT in six patients. They were all detected at BLADE images, thus the sensitivity was 100% (95% CI 68-100%; Fig. 5). However, on HASTE, VIBE and FLASH sequences, consolidation was missed in one patient. There was no false positive for consolidation on MRI.

Other pulmonary abnormalities

Nine atelectases were detected in seven patients and all of these could be demonstrated at MRI (100%; 95% CI 66–100%).

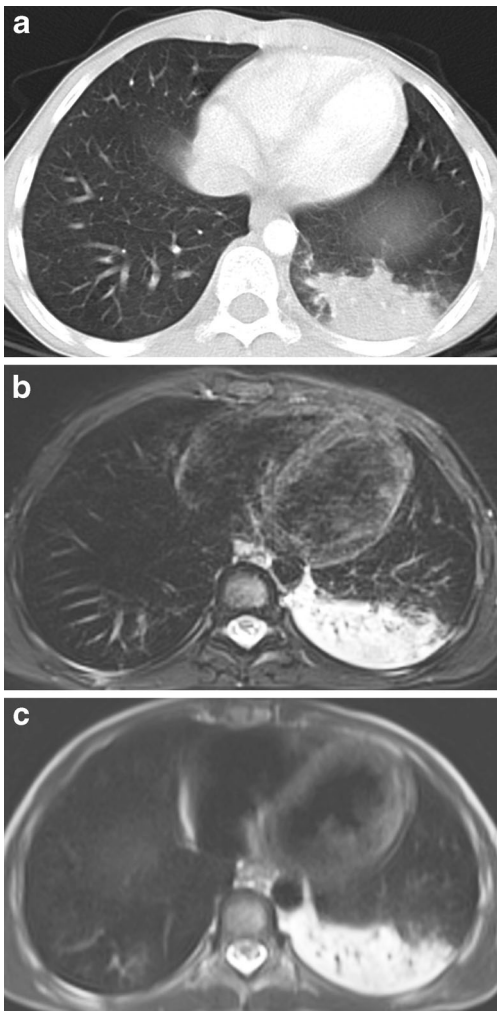

Fig. 5 A 9-year-old boy with acute lymphoblastic leukemia. **a** Transverse thin-section CT image shows consolidation in the left lower lobe. The consolidation is shown both on corresponding transverse T2-weighted spin echo with periodically rotated k space trajectory (**b**) and on transverse T2-weighted half-Fourier single-shot turbo spin echo (**c**)

There was pleural effusion in five patients at MRI. In four patients, all 12 lymph nodes were detected at MRI. In addition, in one patient, three more mediastinal lymph nodes were shown on MRI.

Discussion

MRI seems to be a promising imaging modality for the evaluation of pulmonary infections in immunocompromised children.

The comparison between MRI and CT in our cohort showed an overall diagnostic accuracy of 80.9% for MRI. Of 202 nodules detected with CT, only 157 (77.7%) were depicted with MRI. All nodules larger than 5 mm were detected with MRI. BLADE images and HASTE sequences displayed 100% sensitivity for the detection of such nodules. The highest sensitivity for the detection of nodules smaller than 5 mm was observed for BLADE (69.2%). Performance of the HASTE sequence to detect nodules smaller than 5 mm was surprisingly low (37.7%). In the previous literature, these two fast sequences with rapid acquisition times were defined as useful in lung MRI. Sodhi et al. [22] performed a study about diagnostic utility of MRI with a protocol including BLADE, HASTE, VIBE and steady-state free precession sequences in children. They also found BLADE images and HASTE sequences most sensitive in detecting nodules. In a study by Eibel et al. [9] performed with half-Fourier single-shot turbo spin echo, the sensitivity of MRI in detection of nodules larger than 10 mm was found to be 100% and overall sensitivity was 72%.

Chest radiographs provide little information at early stages of invasive fungal disease because of the high incidence of normal or nonspecific findings [23]. Chest CT is the most useful radiologic examination in invasive fungal disease [19]. On the other hand, being a radiation-free method, pulmonary MRI has become a promising alternative recently. The major problems concerning pulmonary MRI (mainly due to the low proton density of normal lung parenchyma) are susceptibility and cardiac/respiratory motion artifacts. Nevertheless, technical developments in high-performance gradients, phased-array coils and high-field MRI systems have potentially improved its utility in pulmonary diseases [24].

Children are much more susceptible to the harmful effects of radiation than adults, due to increased sensitivity, a longer life span, cumulative doses and a greater dose of radiation per body surface area [25]. Rapid developments in CT technologies have been advocated to minimize radiation doses, including the ALARA (as low as reasonably achievable) principle and low-dose CT protocols. Nevertheless, some patients still have a high risk for radiation including those with DNA repairing deficiency syndromes (ataxia telangiectasia, Bloom syndrome, Fanconi anemia). Hence, this rapid lung MRI protocol can be used for this group of patients.

Yan et al. [10] studied the role of lung MRI in immunocompromised adults with invasive fungal infection with a protocol including five pulse sequences. Spectral-specific inversion recovery sequences were the most sensitive for detecting invasive fungal infection lesions. Spectral fat saturation was explained to provide high image quality and pronounced signal in tissue with active inflammation. We also applied fat saturation on BLADE images. This may be one of the causes for BLADE to have higher sensitivity in detecting pulmonary abnormalities.

The majority of the false-positive findings for the nodules were in group 1 nodules. Also four nodules were defined as group 2 in HASTE whereas they were identified as group 1 on CT images. Likewise, in another patient, the total number of nodules was similar with CT whereas six nodules were defined as group 2 at BLADE images and HASTE sequences butidentified as group 1 on CT images. We attributed the fact that nodules smaller than 5 mm were misinterpreted as larger on MR images to blurring and respiratory artifacts. Regardless of this, most pulmonary abnormalities were disseminated, thus the false-positive or false-negative findings did not ultimately alter treatment. However; small and nonspecific nodules, i.e. without cavitation or halo, can be seen in normal children. The majority of these lesions represent infection/inflammation, scarring or microatelectasis.

In 20 patients with ground-glass opacities in CT, MRI was positive only in 16 (80%); BLADE images and HASTE sequences achieved the same sensitivities. VIBE and FLASH sequences were negative in all 16 patients. In three patients, ground-glass opacities were found on MRI without any correlation with CT, possibly due to blurring artifacts misinterpreted as ground-glass opacity area. In MRI, ghost and blurring artifacts may resemble ground-glass area; hence, the specificity is lower than CT [9].

In our patients, the detection rate for consolidation with MRI or CT was identical. For consolidation, BLADE showed a sensitivity of 100%. The HASTE sequence achieved less favorable sensitivity (87.5%) than the BLADE for consolidation. There was no false-positive or miscalled image in MR examination in terms of consolidation. The detection rates for atelectasis, pleural effusion and lymph nodes were identical for MRI and CT.

Based on the results of our study, lung MRI can be used for the detection of nodules larger than 5 mm, consolidation, atelectasis, pleural effusions and lymph nodes. In addition, T2-BLADE images and T2-HASTE sequences are helpful for detecting lung parenchymal findings in children with pulmonary infections. Total scan time for these two sequences was approximately 10 min, which can reduce the need for sedation or anesthetic support in children. Ultrashort-echo time pulse sequences with even shorter echo times in the range of 0.05–0.20 ms can be produced by use of half radiofrequency excitations with radial mapping from the center of k-space, have echo timese about 10 to 20 times shorter than the shortest generally available on modern clinical systems. Lung MR images with parenchymal sensitivity can be acquired with these pulse sequences.

Our study had some limitations. We included only 17 children with a wide age range and our patient group has diffuse parenchymal disease, which may affect nodule detection with MRI; therefore, confirmation in larger series of patients is needed. Also, the patients in our series were diagnosed according to the criteria of the European Organization for Research and Treatment of Cancer/Mycosis Study Group [20] without a causative pathogen and were not proven histologically.

Conclusion

Our results indicate that lung MRI is promising for detection of pulmonary abnormalities in immunocompromised children with clinically suspected pulmonary infection. Both the BLADE and HASTE sequences achieved reasonable correspondence with CT.

References

1. Krowka MJ, Rosenaw EC, Hoagland HC (1985) Pulmonary complications of bone marrow transplantation. Chest 87:237–246
2. Tanaka N, Matsumoto T, Miura G et al (2002) HRCT findings of chest complications in patients with leukemia. Eur Radiol 12:1512–1522
3. Koyama H, Ohno Y, Kono A et al (2008) Quantitative and qualitative assessment of non-contrast-enhanced pulmonary MR imaging for management of pulmonary nodules in 161 subjects. Eur Radiol 18:2120–2131
4. Lutterbey G, Gieseke J, von Falkenhausen M et al (2005) Lung MRI at 3.0 T: a comparison of helical CT and high field MRI in the detection of diffuse lung disease. Eur Radiol 15:324–328
5. Bruegel M, Gaa J, Woertler K et al (2007) MRI of the lung: value of different turbo spin-echo, single-shot turbo spin-echo, and 3D gradient-echo pulse sequences for the detection of pulmonary metastases. J Magn Reson Imaging 25:73–81
6. Fink C, Puderbach M, Biederer J et al (2007) Lung MRI at 1.5 and 3 Tesla: observer preference study and lesion contrast using five different pulse sequences. Invest Radiol 42:377–383
7. Puderbach M, Hintze C, Ley S et al (2007) MR imaging of the chest: a practical approach at 1.5 T. Eur J Radiol 64:345–355
8. Attenberger UI, Morelli JN, Henzler T et al (2013) 3 Tesla proton MRI for the diagnosis of pneumonia/lung infiltrates in neutropenic patients with acute myeloid leukemia: initial results in comparison to HRCT. Eur J Radiol 83:e61–e66
9. Eibel R, Herzog P, Dietrich O et al (2006) Pulmonary abnormalities in immunocompromised patients: comparative detection with parallel acquisition MR imaging and thin-section helical CT. Radiology 241:880–891
10. Yan C, Tan X, Wei Q et al (2015) Lung MRI of invasive fungal infection at 3 Tesla: evaluation of five different pulse sequences and

comparison with multidetector computed tomography (MDCT). Eur Radiol 25:550–557
11. Leutner CC, Gieseke J, Lutterbey G et al (2000) MR imaging of pneumonia in immunocompromised patients: comparison with helical CT. AJR Am J Roentgenol 175:391–397
12. Peltola V, Ruuskanen O, Svedström E (2008) Magnetic resonance imaging of lung infections in children. Pediatr Radiol 38:1225–1231
13. Hebestreit A, Schultz G, Trusen A et al (2004) Follow-up of acute pulmonarycomplications in cystic fibrosis by magnetic resonance imaging. Acta Paediatr 93:414–416
14. Wagner M, Böwing B, Kuth R et al (2001) Low field thoracic MRI – a fast and radiation free routine imaging modality in children. Magn Reson Imaging 19:975–983
15. Yikilmaz A, Koc A, Coskun A et al (2011) Evaluation of pneumonia in children: comparison of MRI with fast imaging sequences at 1.5T with chest radiographs. Acta Radiol 52:914–919
16. Gorkem SB, Coskun A, Yikilmaz A et al (2013) Evaluation of pediatric thoracic disorders: comparison of unenhanced fast-imaging-sequence 1.5-T MRI and contrast-enhanced MDCT. AJR Am J Roentgenol 200:1352–1357
17. Montella S, Maglione M, Bruzzese D et al (2012) Magnetic resonance imaging is an accurate and reliable method to evaluate non-cystic fibrosis paediatric lung disease. Respirology 17:87–91
18. Lehrnbecher T, Phillips R, Alexander S et al (2012) Guideline for the management of fever and neutropenia in children with cancer and/or undergoing hematopoietic stem-cell transplantation. J Clin Oncol 30:4427–4438
19. Herbrecht R, Natarajan-Ame S, Letscher-Bru V et al (2004) Invasive pulmonary aspergillosis. Semin Respir Crit Care Med 25:191–202
20. De Pauw B, Walsh TJ, Donnelly JP et al (2008) Revised definitions of invasive fungal disease from the European Organization for Research and Treatment of Cancer/Invasive Fungal Infections Cooperative Group and the National Institute of Allergy and Infectious Diseases Mycoses Study Group (EORTC/MSG) Consensus Group. Clin Infect Dis 46:1813–1821
21. Hansell DM, Bankier AA, MacMahon H et al (2008) Fleischner society: glossary of terms for thoracic imaging. Radiology 246: 697–722
22. Sodhi KS, Khandelwal N, Saxena AK et al (2015) Rapid lung MRI in children with pulmonary infections: time to change our diagnostic algorithms. J Magn Reson Imaging 43:1196–1206
23. Hauggaard A, Ellis M, Ekelund L (2002) Early chest radiography and CT in the diagnosis, management and outcome of invasive pulmonary aspergillosis. Acta Radiol 43:292–298
24. Sieren JC, Ohno Y, Koyama H et al (2010) Recent technological and application developments in computed tomography and magnetic resonance imaging for improved pulmonary nodule detection and lung cancer staging. J Magn Reson Imaging 32:1353–1369
25. Brody AS, Frush DP, Huda W et al (2007) Radiation risk to children from computed tomography. Pediatrics 120:677–682